

Unsteady Laminar Natural Convection from a Non-Isothermal Vertical Cone

B. Pullepu¹, K. Ekambavanan¹, A. J. Chamkha²

¹Department of Mathematics, College of Engineering
Anna University, Chennai, 600025 India
bapujip@yahoo.com; akevanan@annauniv.edu

²Manufacturing Engineering Department
The Public Authority for Applied Education and Training
Shuweikh, 70654 Kuwait
achamkha@yahoo.com

Received: 28.11.2006 **Revised:** 15.01.2007 **Published online:** 12.11.2007

Abstract. Natural convection effects of the numerical solution for unsteady, laminar, free convection flow over an incompressible viscous fluid past a non-isothermal vertical cone with surface temperature $T_w'(x) = T_\infty' + ax^n$ varying as power function of distance from the apex ($x = 0$) is presented here. The dimensionless governing equations of the flow that are unsteady, coupled and non-linear partial differential equations are solved by an efficient, accurate and unconditionally stable finite difference scheme of Crank-Nicolson type. The velocity and temperature fields have been studied for various parameters Prandtl number, semi vertical angle $0^\circ < \phi < 90^\circ$ and n . The local as well as average skin-friction and Nusselt number are also presented and analyzed graphically. The present results are compared with available results in literature and are found to be in good agreement.

Keywords: cone, finite-difference method, heat transfer, natural convection, unsteady.

Nomenclature

a	constant	\overline{Nu}	non-dimensional average Nusselt number
f''	local skin-friction in [5, 15]	n	exponent in power law variation in surface temperature
Gr_L	Grashof number	Pr	Prandtl number
Gr_L^*	modified Grashof number ($Gr_L \cos \phi$)	R	dimensionless local radius of the cone
g	acceleration due to gravity	r	local radius of the cone
L	reference length	T'	temperature
Nu_x	local Nusselt number	T	dimensionless temperature
\overline{Nu}_L	average Nusselt number		
Nu_X	non-dimensional local Nusselt number		

t'	time	X	dimensionless spatial co-ordinate
t	dimensionless time	x	spatial co-ordinate along cone generator
U	dimensionless velocity in X -direction	Y	dimensionless spatial co-ordinate along the normal to the cone generator
u	velocity component in x -direction	y	spatial co-ordinate along the normal to the cone generator
V	dimensionless velocity in Y -direction		
v	velocity component in y -direction		

Greek symbols

α	thermal diffusivity	μ	dynamic viscosity
β	volumetric thermal expansion	ν	kinematic viscosity
Δt	dimensionless time-step	τ_x	local skin-friction
ΔX	dimensionless finite difference grid size in X -direction	τ_X	dimensionless local skin-friction
ΔY	dimensionless finite difference grid size in Y -direction	$\bar{\tau}_L$	average skin-friction
ϕ	semi vertical angle of the cone	$\bar{\tau}$	dimensionless average skin-friction
		$-\theta'(0)$	local Nusselt number in [5, 15]

Subscripts

w	condition on the wall	∞	free stream condition
-----	-----------------------	----------	-----------------------

1 Introduction

Natural convection flows under influence of gravitational force have been investigated most extensively because they occur frequently in nature as well as in science and engineering applications. When a heated surface is in contact with the fluid, the result of temperature difference causes buoyancy force, which induces the natural convection. The atmospheric circulation with all its hurricanes, blizzards and monsoons are essentially driven by natural convection. Mainly, these types of heat transfer problems deal with the design of spacecrafts, nuclear reactor, solar power collectors, power transformers, steam generators etc.

Since 1953, several authors have developed similarity solutions for axi-symmetrical problems for natural convection laminar flow over a vertical cone in steady state. Merk and Prins [1, 2] developed the general relation for similar solutions on iso-thermal axi-symmetric forms and they showed that the vertical cone has such a solution in steady state. Braun et al. [3] obtained similar solutions for isothermal axi-symmetric bodies (i.e., cone, parabolic-nosed, flat-nosed bodies) with closed lower ends, and integral methods are used for obtaining heat transfer results for a wide range of Prandtl numbers. These authors also presented the results obtained by numerically integrating the differential equations with including Prandtl number of 0.72 and concluded; the body shape influences the heat transfer strongly for lower Prandtl numbers. Further, Hering and Grosh [4] showed the similarity solutions exist for steady free convection flow over a vertical cone with variable surface temperature and it varies as power function of distance from apex along the cone

ray. Numerical solutions of the transformed boundary layer equations are obtained for both isothermal and linear surface temperature with Prandtl number 0.7. They noticed from the velocity and temperature profiles that the dimensionless tangential-flow function for the iso-thermal cone attains 22 % greater than that for the cone with linear surface temperature distribution. Hering [5] extended the problem of Hering and Grosh [4] for low Prandtl number fluids, and obtained numerical solutions for liquid metals and concluded that the thermal boundary layer thickness is more for low Prandtl number fluids. Sparrow et al. [6] observed that the boundary layer thickness in the case of isothermal vertical plate for air ($Pr = 0.733$) is comparatively 14.5 times less than that for liquid sodium ($Pr = 0.003$). Roy [7] extended the work of Hering and Grosh [4] for high Prandtl number fluids, and derived expressions for local skin-friction and Nusselt numbers. Also, Alamgir [8] has investigated the overall heat transfer in laminar natural convection from vertical cones using the integral method. Pop and Takhar [9] have studied the compressibility effects in laminar free convection from a vertical cone. Kumari and Pop et al. [10] who investigated the steady mixed convection flow over a vertical cone for two values of the Pr , namely $Pr = 0.733$ (air) and $Pr = 6.7$ (water) However, these authors have considered only the case of assisting flow. Recently, Pop and Grosan et al. [11] analyzed the steady laminar mixed convection boundary-layer flow over a vertical isothermal cone for fluids of any Pr for the both cases of buoyancy assisting and buoyancy opposing flow conditions. The resulting non-similarity boundary-layer equations are solved numerically using the Keller-box scheme for fluids of any Pr from very small to extremely large values ($0.001 \leq Pr \leq 10000$).

Further, Gorla and Startman [12] considered the analysis of transverse curvature effect on axi-symmetric free convection boundary layer flow of water at 4°C past a slender vertical cone and observed the heat transfer rate increases with the increasing transverse curvature. Also, Kuiken [13] have considered the case of a slender cone where the transverse curvature effect is considered. The transformed boundary-layer equations are non-similar, and these equations were solved in terms of series expansion of the transverse curvature variable. Watanabe [14] solved a non-similar free convection boundary layer flow with constant wall temperature and uniform suction/injection over a cone and presented numerical results for various suction/injection and vertical angle parameters. Recently, Hossain and Paul [15] studied the non-similarity solutions for the laminar free convection from a vertical permeable cone with non-uniform surface temperature. Using a finite difference method, a series solution method and asymptotic solution method, the solutions have been obtained for the non-similarity boundary layer equations. Takhar and Chamkha et al. [16] investigated the effect of thermo physical quantities on the free convection flow of gases over iso-thermal vertical cone in steady state, in which thermal conductivity, dynamic viscosity and specific heat at constant pressure were to be assumed a power law variation with absolute temperature. They concluded the heat transfer increases with suction and decreases with injection. Further, solutions of the transient free convection flow problems over a vertical/started vertical plate and inclined plate/vertical cylinder have been obtained by Takhar and Ganesan et al. [17], Muthucumaraswamy and Ganesan [18], Ekambavanan and Ganesan [19], Ganesan and Rani [20] using finite difference method.

The investigation, namely unsteady laminar natural convection flow past a non-isothermal vertical cone has not received any attention in literature. Hence, the present work-studies and deals with the laminar free convection flow over a non-isothermal vertical cone. The governing boundary layer equations are solved by an implicit finite difference scheme of Crank-Nicolson type with Pr , ϕ and n as controlling parameters. In order to check the accuracy of our numerical results, the present results are computed at $X = 1.0$ by considering modified Grashof number $Gr_L^* = Gr_L \cos \phi = \frac{g\beta \cos \phi (T_w' - T_\infty') L^3}{\nu^2}$ and results are compared with the available results of Hering and Grosh [4], Hering [5] and Hossain [15].

2 Mathematical analysis

An axi-symmetric unsteady laminar free convection of a viscous incompressible flow past a vertical cone with variable temperature $T_w'(x) = T_\infty' + ax^n$ on the surface is considered. It is assumed that the viscous dissipation effects are negligible. It is also assumed that the cone surface and the surrounding fluid which is at rest are at the same temperature T_∞' . Then at time $t' > 0$, the temperature of the cone surface is suddenly raised to $T_w'(x) = T_\infty' + ax^n$ and it is maintained. The co-ordinate system is chosen (as shown in Fig. 1) such that measures the distance along surface of the cone from

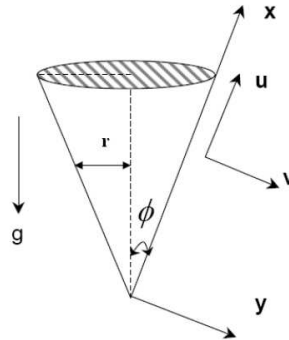


Fig. 1. Physical model and co-ordinate system.

the apex ($x = 0$) and y measures the distance normally outward. Here ϕ is the semi vertical angle of the cone and r is the local radius of the cone. The fluid properties are assumed constant except for density variations, which induce buoyancy force term in the momentum equation. The governing boundary layer equations of continuity, momentum and energy under Boussinesq approximation are as follows:

Equation of continuity:

$$\frac{\partial(ur)}{\partial x} + \frac{\partial(vr)}{\partial y} = 0, \tag{1}$$

equation of momentum:

$$\frac{\partial u}{\partial t} + u \frac{\partial u}{\partial x} + v \frac{\partial u}{\partial y} = g\beta \cos \phi (T' - T'_\infty) + \nu \frac{\partial^2 u}{\partial y^2}, \quad (2)$$

equation of energy:

$$\frac{\partial T'}{\partial t'} + u \frac{\partial T'}{\partial x} + v \frac{\partial T'}{\partial y} = \alpha \frac{\partial^2 T'}{\partial y^2}. \quad (3)$$

The initial and boundary conditions are

$$\begin{aligned} t' \leq 0: & \quad u = 0, \quad v = 0, \quad T' = T'_\infty && \text{for all } x, y, \\ t' > 0: & \quad u = 0, \quad v = 0, \quad T'(x) = T'_\infty + ax^n && \text{at } y = 0, \\ & \quad u = 0, \quad T' = T'_\infty && \text{at } x = 0, \\ & \quad u \rightarrow 0, \quad T' \rightarrow T'_\infty && \text{as } y \rightarrow \infty. \end{aligned} \quad (4)$$

Local skin-friction and local Nusselt number are given respectively by

$$\tau_x = \mu \left(\frac{\partial u}{\partial y} \right)_{y=0}, \quad (5)$$

$$Nu_x = \frac{-x \left(\frac{\partial T'}{\partial y} \right)_{y=0}}{T'_w - T'_\infty}. \quad (6)$$

Average skin-friction is given by

$$\bar{\tau}_L = \frac{2\mu}{L^2} \int_0^L x \left(\frac{\partial u}{\partial y} \right)_{y=0} dx. \quad (7)$$

Average heat transfer co-efficient over cone surface is

$$\bar{h} = \frac{-2k}{L^2} \int_0^L x \frac{\left(\frac{\partial T'}{\partial y} \right)_{y=0}}{T'_w - T'_\infty} dx, \quad (8)$$

then average Nusselt number is

$$\bar{Nu}_L = \frac{\bar{h}L}{k} = \frac{-2}{L} \int_0^L x \frac{\left(\frac{\partial T'}{\partial y} \right)_{y=0}}{T'_w - T'_\infty} dx. \quad (9)$$

Using the following non-dimensional quantities:

$$\begin{aligned} X &= \frac{x}{L}, \quad Y = \frac{y}{L} (Gr_L)^{\frac{1}{4}}, \quad R = \frac{r}{L}, \quad \text{where } r = x \sin \phi, \\ V &= \frac{vL}{\nu} (Gr_L)^{-\frac{1}{4}}, \quad U = \frac{uL}{\nu} (Gr_L)^{-\frac{1}{2}}, \quad t = \frac{\nu t'}{L^2} (Gr_L)^{\frac{1}{2}}, \\ T &= \frac{T' - T'_\infty}{T'_w(L) - T'_\infty}, \quad Gr_L = \frac{g\beta(T'_w(L) - T'_\infty)L^3}{\nu^2}, \quad Pr = \frac{\nu}{\alpha}. \end{aligned} \quad (10)$$

Equations (1), (2) and (3) are reduced to the following non-dimensional form:

$$\frac{\partial(UR)}{\partial X} + \frac{\partial(VR)}{\partial Y} = 0 \quad \left(\text{or} \quad \frac{\partial(U)}{\partial X} + \frac{\partial(V)}{\partial Y} + \frac{U}{X} = 0 \right), \quad (11)$$

$$\frac{\partial U}{\partial t} + U \frac{\partial U}{\partial X} + V \frac{\partial U}{\partial Y} = T \cos \phi + \frac{\partial^2 U}{\partial Y^2}, \quad (12)$$

$$\frac{\partial T}{\partial t} + U \frac{\partial T}{\partial X} + V \frac{\partial T}{\partial Y} = \frac{1}{Pr} \frac{\partial^2 T}{\partial Y^2}. \quad (13)$$

The corresponding initial and boundary conditions in non-dimensional quantities are given by

$$\begin{aligned} t \leq 0: \quad & U = 0, \quad V = 0, \quad T = 0 \quad \text{for all } X, Y, \\ t > 0: \quad & U = 0, \quad V = 0, \quad T = X^n \quad \text{at } Y = 0, \\ & U = 0, \quad T = 0 \quad \text{at } X = 0, \\ & U \rightarrow 0, \quad T \rightarrow 0 \quad \text{as } Y \rightarrow \infty. \end{aligned} \quad (14)$$

Local skin-friction and local Nusselt number in non-dimensional quantities are

$$\tau_X = Gr_L^{\frac{3}{4}} \left(\frac{\partial U}{\partial Y} \right)_{Y=0}, \quad (15)$$

$$Nu_X = \frac{X}{T_{Y=0}} \left(\frac{-\partial T}{\partial Y} \right)_{Y=0} Gr_L^{\frac{1}{4}}. \quad (16)$$

Average skin-friction and average Nusselt number in non-dimensional quantities are

$$\bar{\tau} = 2Gr_L^{\frac{3}{4}} \int_0^1 x \left(\frac{\partial U}{\partial Y} \right)_{y=0} dX, \quad (17)$$

$$\bar{Nu} = 2Gr_L^{\frac{1}{4}} \int_0^1 \frac{X}{T_{Y=0}} \left(\frac{-\partial T}{\partial Y} \right)_{Y=0} dX. \quad (18)$$

3 Solution procedure

The unsteady non-linear coupled partial differential equations (11), (12) and (13) with the initial and boundary conditions (14) are solved by employing a finite difference scheme of Crank-Nicholson type which is discussed by many authors Muthucumaraswamy and Ganesan [18], Ganesan and Rani [20], Ekambavanan and Ganesan [19], Takhar and Ganesan et al. [17]. The finite difference equations corresponding to the equations are given by

$$\begin{aligned} & \frac{U_{i,j}^{k+1} - U_{i-1,j}^{k+1} + U_{i,j}^k - U_{i-1,j}^k + U_{i,j-1}^{k+1} - U_{i-1,j-1}^{k+1} + U_{i,j-1}^k - U_{i-1,j-1}^k}{4\Delta X} \\ & + \frac{V_{i,j}^{k+1} - V_{i,j-1}^{k+1} + V_{i,j}^k - V_{i,j-1}^k}{2\Delta Y} + \frac{U_{i,j}^{k+1} + U_{i,j-1}^{k+1} + U_{i,j}^k + U_{i,j-1}^k}{4i\Delta X} = 0, \end{aligned} \quad (19)$$

$$\begin{aligned}
 & \frac{U_{i,j}^{k+1} - U_{i,j}^k}{\Delta t} + U_{i,j}^k \frac{U_{i,j}^{k+1} - U_{i-1,j}^{k+1} + U_{i,j}^k - U_{i-1,j}^k}{2\Delta X} \\
 & \quad + V_{i,j}^k \frac{U_{i,j+1}^{k+1} - U_{i,j-1}^{k+1} + U_{i,j+1}^k - U_{i,j-1}^k}{4\Delta Y} \\
 & = \frac{T_{i,j}^{k+1} + T_{i,j}^k}{2} \cos \phi + \frac{U_{i,j-1}^{k+1} - 2U_{i,j}^{k+1} + U_{i,j+1}^{k+1} + U_{i,j-1}^k - 2U_{i,j}^k + U_{i,j+1}^k}{2(\Delta Y)^2},
 \end{aligned} \tag{20}$$

$$\begin{aligned}
 & \frac{T_{i,j}^{k+1} - T_{i,j}^k}{\Delta t} + U_{i,j}^k \frac{T_{i,j}^{k+1} - T_{i-1,j}^{k+1} + T_{i,j}^k - T_{i-1,j}^k}{2\Delta X} \\
 & \quad + V_{i,j}^k \frac{T_{i,j+1}^{k+1} - T_{i,j-1}^{k+1} + T_{i,j+1}^k - T_{i,j-1}^k}{4\Delta Y} \\
 & = \frac{1}{Pr} \frac{T_{i,j-1}^{k+1} - 2T_{i,j}^{k+1} + T_{i,j+1}^{k+1} + T_{i,j-1}^k - 2T_{i,j}^k + T_{i,j+1}^k}{2(\Delta Y)^2}.
 \end{aligned} \tag{21}$$

Here the region of integration is considered as a rectangle with $X_{max} = 1$ and $Y_{max} = 20$ where Y_{max} corresponds to $Y = \infty$ which lies very well outside both the momentum and thermal boundary layers. The maximum of Y was chosen as 20, after some preliminary investigation so that the last two boundary conditions of (14) are satisfied within the tolerance limit 10^{-5} . The mesh sizes have been fixed as $\Delta X = 0.05$, $\Delta Y = 0.05$ with time step $\Delta t = 0.01$. The computations are carried out first by reducing the spatial mesh sizes by 50% in one direction, and later in both directions by 50%. The results are compared. It is observed that, in all cases, the results differ only in the fifth decimal place. Hence, the choice of the mesh sizes seems to be appropriate. The co-efficient of $U_{i,j}^k$ and $V_{i,j}^k$ appearing in the finite-difference equations are treated as constants at any one-time step. Here i designates the grid point along the X -direction, j along the Y -direction and k along the time t . The values of U , V and T are known at all grid points when $t = 0$ from the initial conditions.

The computations of U , V and T at a time level $(k + 1)$, using the values at previous time level k are carried out as follows. The finite-difference equation (21) at every internal nodal point on a particular i -level constitutes a tri-diagonal system of equations and is solved by Thomas algorithm as discussed in Carnahan et al. [21]. Thus, the values of T known at every nodal point at a particular i at $(k + 1)^{th}$ time level. Similarly, the values of U are calculated from equation (20), and finally the values of V are calculated explicitly by using equation (19) at every nodal point on a particular i -level at $(k + 1)^{th}$ time level. In a similar manner, computations are carried out by moving along i -direction. After computing values corresponding to each i at a time level, the values at the next time level are determined in a similar manner. Computations are repeated until steady state is reached. The steady state solution is assumed to have been reached when the absolute difference between the values of the velocity U , as well as temperature T at two consecutive time steps are less than 10^{-5} at all grid points.

The scheme is unconditionally stable. The local truncation error is $O(\Delta t^2 + \Delta Y^2 + \Delta X)$ and it tends to zero as $\Delta t, \Delta Y$ and ΔX tend to zero. Hence, the scheme is compatible. Stability and compatibility ensure the convergence.

4 Results and discussion

In order to prove the accuracy of our numerical results, the present results in steady state at $X = 1.0$, $Pr = 0.7$, $\eta = Y$ and considering $Gr_L^* = Gr_L \cos \phi = \frac{g\beta \cos \phi (T_w' - T_\infty') L^3}{\nu^2}$ are compared with available similarity solutions in the literature. In Figs. 2(a) and 2(b), the velocity and temperature profiles of isothermal and non-isothermal vertical cone are compared with similarity solutions of Hering and Grosh [4] in steady state and found to be in excellent agreement. In addition, local skin-friction τ_X and local Nusselt number Nu_X values for different Prandtl number and exponent n are compared with the results of Hering [5] in Tables 1 and 2, respectively. It is observed that the results are in good agreement with each other for small values of n . There is small deviation with these results for large values of n and the deviation increases with n . Also, present values of local skin-friction τ_X and local Nusselt number Nu_X values for different Prandtl number and exponent value when are compared with the recent results, non-similarity solution of Hossain [15] in Table 3. Finally, Pop and Takhar [9] results are for incompressible fluid same as those of Hering and Grosh [4] results. Hence, present results well agree with the results of Pop and Thakar [9] for incompressible fluid.

In Figs. 3–5, transient velocity and temperature profiles are shown at $X = 1.0$, with various parameters Pr, n and ϕ . The values of t with star symbols (*) denote the time taken to reach steady state. In Fig. 3(a), transient velocity profiles are shown for different angles with $Pr = 0.71$ and $n = 0.2$. When ϕ increases, near the cone apex, it leads to a decrease in the impulsive force along the cone surface. Hence, the difference between temporal maximum velocity values and steady state values decreases with increasing the values of ϕ . The tangential component of buoyancy force reduces as the semi vertical angle increases. This causes the velocity to reduce as angle ϕ increases. The momentum boundary layer becomes thick, and the time taken to reach steady state increases for increasing ϕ .

In Fig. 3(b), transient temperature profiles are shown for different angles with $Pr = 0.71$ and $n = 0.2$. It is observed the temperature and boundary layer thickness increase with increasing ϕ . The difference between temporal maximum temperature values and steady state values decrease with increasing ϕ .

In Figs. 4(a) and 4(b), transient velocity and temperature profiles are plotted for various values of Pr with $\phi = 15^\circ$ and $n = 0.2$. Viscous force increases and thermal diffusivity reduces with increasing Pr , causes a reduction in the velocity and temperature as expected. It is observed from the figures that the difference between temporal maximum values and steady state values are reduced when Pr increases. It is also noticed the time taken to reach steady state increases and thermal boundary layer thickness reduces with increasing Pr . It is also clear from the Fig. 4(a), the momentum boundary layer thickness increases with the increase of Pr from unity.

Table 1. Comparison of steady state local skin-friction results at $X = 1.0$ with those of Hering [5]

n	Hering [5]			Present values			Hering [5]			Present values		
	$f''(0)$	$f''(0)\sqrt{Pr}$	$\tau_x/(Gr_L^*)^{3/4}$	$f''(0)$	$f''(0)\sqrt{Pr}$	$\tau_x/(Gr_L^*)^{3/4}$	$f''(0)$	$f''(0)\sqrt{Pr}$	$\tau_x/(Gr_L^*)^{3/4}$	$f''(0)$	$f''(0)\sqrt{Pr}$	$\tau_x/(Gr_L^*)^{3/4}$
	$Pr = 0.03$						$Pr = 0.1$					
0	7.185	1.2444	1.2406	3.466	1.0960	1.0932	3.466	1.0960	1.0932	3.466	1.0960	1.0932
0.2	6.928	1.1999	1.1973	3.353	1.0603	1.0589	3.353	1.0603	1.0589	3.353	1.0603	1.0589
1	6.174	1.0693	1.0703	3.019	0.9545	0.9567	3.019	0.9545	0.9567	3.019	0.9545	0.9567
2	5.582	0.9668	0.9709	2.749	0.8693	0.8736	2.749	0.8693	0.8736	2.749	0.8693	0.8736
4	4.892	0.8473	0.8568	2.425	0.7668	0.7757	2.425	0.7668	0.7757	2.425	0.7668	0.7757
8	4.197	0.7269	0.7864	2.091	0.6612	0.6778	2.091	0.6612	0.6778	2.091	0.6612	0.6778
n	$Pr = 0.7$						$Pr = 1.0$					
0	0.9796	0.8195	0.8163	0.7694	0.7694	0.7660	0.7694	0.7694	0.7660	0.7694	0.7694	0.7660
0.2	0.9513	0.7959	0.7937	0.7475	0.7475	0.7451	0.7475	0.7475	0.7451	0.7475	0.7475	0.7451
1	0.8663	0.7248	0.7255	0.6815	0.6815	0.6819	0.6815	0.6815	0.6819	0.6815	0.6815	0.6819
2	0.7962	0.6661	0.6684	0.6270	0.6270	0.6289	0.6270	0.6270	0.6289	0.6270	0.6270	0.6289
4	0.7096	0.5937	0.5993	0.5596	0.5596	0.5645	0.5596	0.5596	0.5645	0.5596	0.5596	0.5645
8	0.6172	0.5164	0.5277	0.4872	0.4872	0.4977	0.4872	0.4872	0.4977	0.4872	0.4872	0.4977

Table 2. Comparison of steady state local Nusselt number values at $X = 1.0$ with those of Hering [5]

n	Hering [5]			Present values			Hering [5]			Present values		
	$-\theta'(0)$	$-\theta'(0)\sqrt{Pr}$	$Nu_x/(Gr_L^*)^{1/4}$	$-\theta'(0)$	$-\theta'(0)\sqrt{Pr}$	$Nu_x/(Gr_L^*)^{1/4}$	$-\theta'(0)$	$-\theta'(0)\sqrt{Pr}$	$Nu_x/(Gr_L^*)^{1/4}$	$-\theta'(0)$	$-\theta'(0)\sqrt{Pr}$	$Nu_x/(Gr_L^*)^{1/4}$
	$Pr = 0.03$						$Pr = 0.1$					
0	0.7185	0.12440	0.1258	0.6683	0.2113	0.2121	0.6683	0.2113	0.2121	0.6683	0.2113	0.2121
0.2	0.7726	0.13380	0.1352	0.7159	0.2263	0.2271	0.7159	0.2263	0.2271	0.7159	0.2263	0.2271
1	0.9415	0.16307	0.1623	0.8663	0.2739	0.2733	0.8663	0.2739	0.2733	0.8663	0.2739	0.2733
2	1.0890	0.18860	0.1879	0.9919	0.3136	0.3120	0.9919	0.3136	0.3120	0.9919	0.3136	0.3120
4	1.2870	0.22290	0.2174	1.1650	0.3684	0.3620	1.1650	0.3684	0.3620	1.1650	0.3684	0.3620
8	1.5330	0.26550	0.2522	1.3810	0.4367	0.4185	1.3810	0.4367	0.4185	1.3810	0.4367	0.4185
n	$Pr = 0.7$						$Pr = 1.0$					
0	0.5392	0.4511	0.4554	0.5104	0.5104	0.5157	0.5104	0.5104	0.5157	0.5104	0.5104	0.5157
0.2	0.5730	0.4794	0.4833	0.5148	0.5148	0.5465	0.5148	0.5148	0.5465	0.5148	0.5148	0.5465
1	0.6777	0.5670	0.5684	0.6389	0.6389	0.6406	0.6389	0.6389	0.6406	0.6389	0.6389	0.6406
2	0.7693	0.6436	0.6412	0.7240	0.7240	0.7213	0.7240	0.7240	0.7213	0.7240	0.7240	0.7213
4	0.8945	0.7484	0.7374	0.8406	0.8406	0.8285	0.8406	0.8406	0.8285	0.8406	0.8406	0.8285
8	1.0530	0.8810	0.8489	0.9889	0.9889	0.9535	0.9889	0.9889	0.9535	0.9889	0.9889	0.9535

Table 3. Comparison of steady state local skin-friction and local Nusselt number values at $X = 1.0$ with those of Hossain [15] when $n = 0.5$ and suction is zero.

$n = 0.5$	Local skin-function		Local Nusselt number	
	Hossain values	Present values	Hossain values	Present values
Pr	$f''(0)$	$\tau_X / (Gr_L^*)^{3/4}$	$-\theta'(0)$	$Nu_X / (Gr_L^*)^{1/4}$
0.01	1.23231	1.224	0.08828	0.0914
0.05	1.09069	1.0922	0.183	0.1829
0.1	1.01332	1.015	0.24584	0.2466

In Figs. 5(a) and 5(b), transient velocity and temperature profiles are shown for various values of n with $Pr = 0.71$ and $\phi = 15^\circ$. Impulsive forces are reduced along the surface of the cone near the vertex for increasing values of n . Due to this, the difference between temporal maximum values and steady state values reduce. It is also observed that as n increases, velocity and temperature reduce and the time taken to reach steady state value increases.

Once velocity and temperature profiles are studied, it is interesting to study the local as well as the average skin-friction, and the rate of heat transfer in steady and transient state. The derivatives involved in equations (15)–(18) are obtained using five-point approximation formulae and then the integrals are evaluated using Newton-Cotes closed integration formula. The local skin-friction τ_X and local Nusselt number Nu_X for different values of ϕ , at various positions on the surface of the cone ($X = 0.25$ and 1.0) in the transient period are shown in Fig. 6(a) and 6(b) respectively. It is observed from the figures local skin-friction τ_X and local Nusselt number Nu_X values decrease with increasing angle ϕ . It is observed this effect is less near the cone apex.

The local skin-friction τ_X and local Nusselt number Nu_X values for different values of Pr , at various positions on the surface of the cone ($X = 0.25$ and 1.0) in the transient period are shown in Fig. 7(a) and 7(b) respectively. It is observed from the figures local skin-friction τ_X and local Nusselt number Nu_X decreases with increasing Pr and also clear from the figures decreasing rate of τ_X and Nu_X increases when the distance increase from the cone vertex along the surface of the cone.

The variation of the local skin-friction τ_X and the local Nusselt number Nu_X in the transient period at various positions on the surface of the cone ($X = 0.25$ and 1.0) and for different values of n , are shown in Figs. 8(a) and 8(b). It is observed from Fig. 8(a) that the local skin-friction decreases with increasing n and the effect of n over the local skin-friction τ_X is more near the apex of the cone and reduces gradually with increasing the distance along the surface of the cone from the apex. From Fig. 8(b), it is noticed that near the apex, local Nusselt number Nu_X reduces with increasing n , but that trend is slowly changed and reversed as distance increases along the surface from apex.

The influence of average skin-friction $\bar{\tau}$ is more in transient period for smaller values of ϕ or lower values of Pr or smaller values of n which is shown in Figs. 9(a), 9(b), displays influence of average Nusselt number \bar{Nu} in transient period for various values of Pr, ϕ and n . It is clear \bar{Nu} is more for smaller values of ϕ and large values of Pr . Also, observed that there is no significant influence of n over the average Nusselt number.

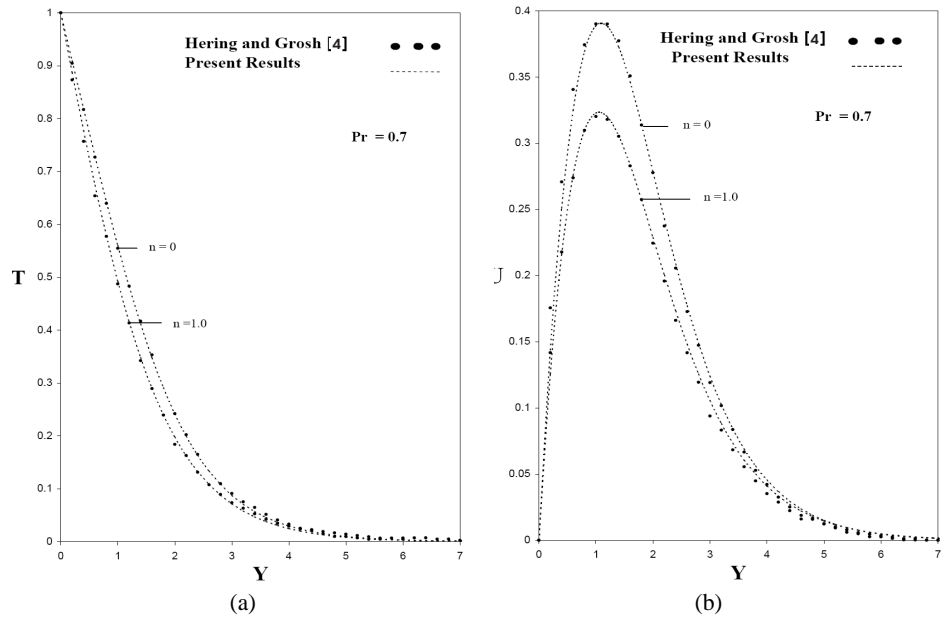


Fig. 2. Comparison of steady state temperature profiles (a) and velocity profiles (b) at $X = 1.0$.

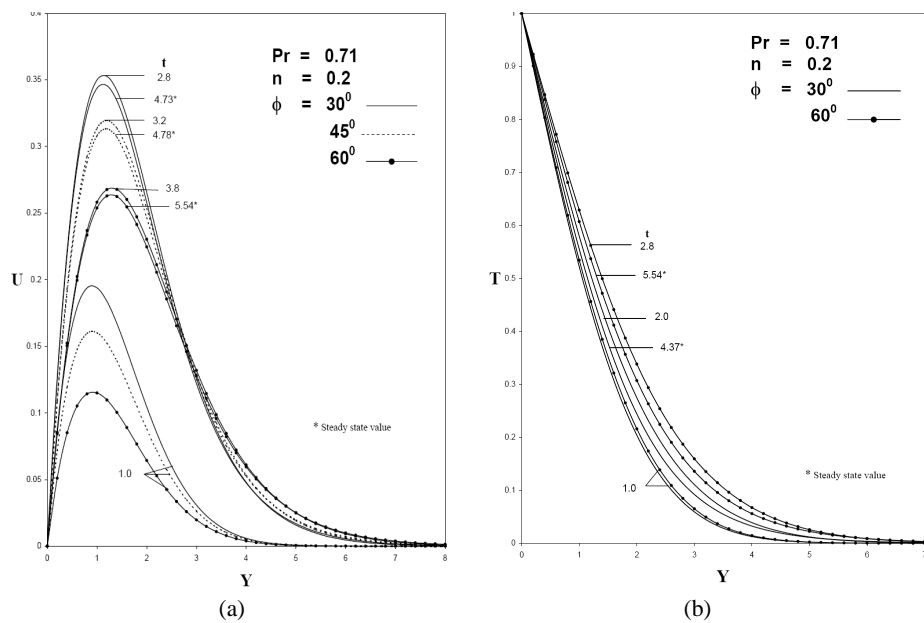


Fig. 3. Transient velocity profiles (a) and transient temperature profiles (b) at $X = 1.0$ for different values of ϕ .

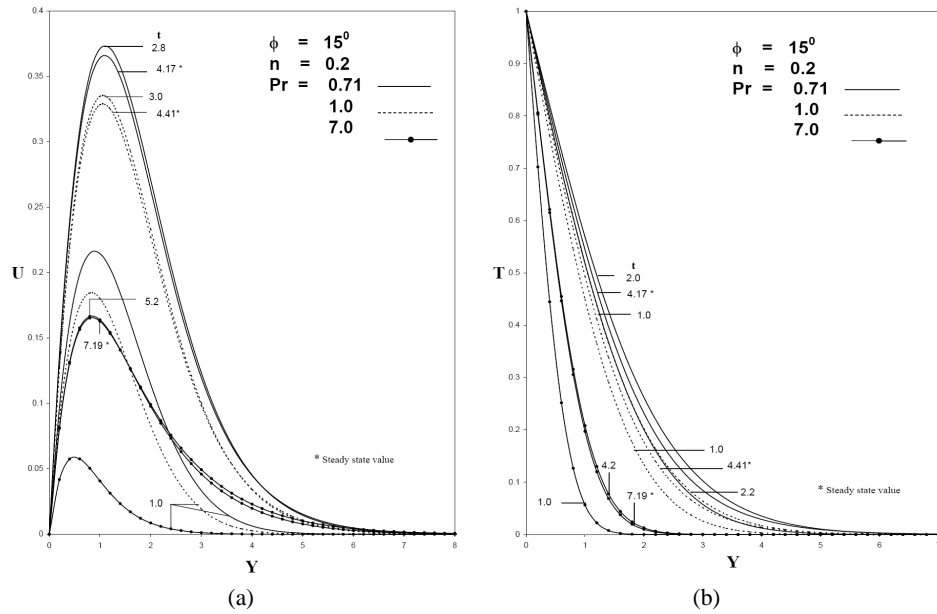


Fig. 4. Transient velocity profiles (a) and transient temperature profiles (b) at $X = 1.0$ for different values of Pr .

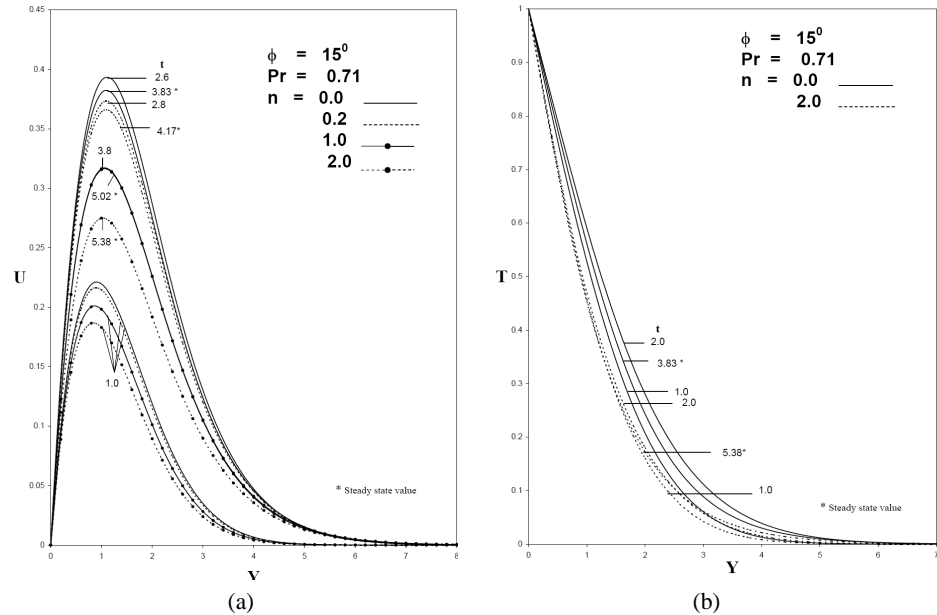


Fig. 5. Transient velocity profiles (a) and transient temperature profiles (b) at $X = 1.0$ for different values of n .

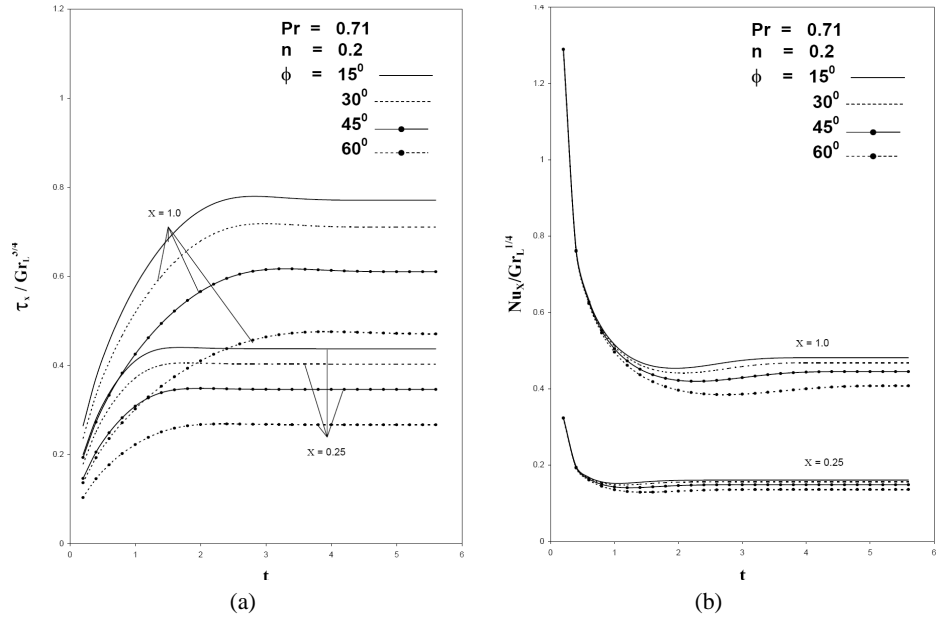


Fig. 6. Local skin friction (a) and local Nusselt number (b) at $X = 0.25$ and 1.0 for different values of ϕ in transient period.

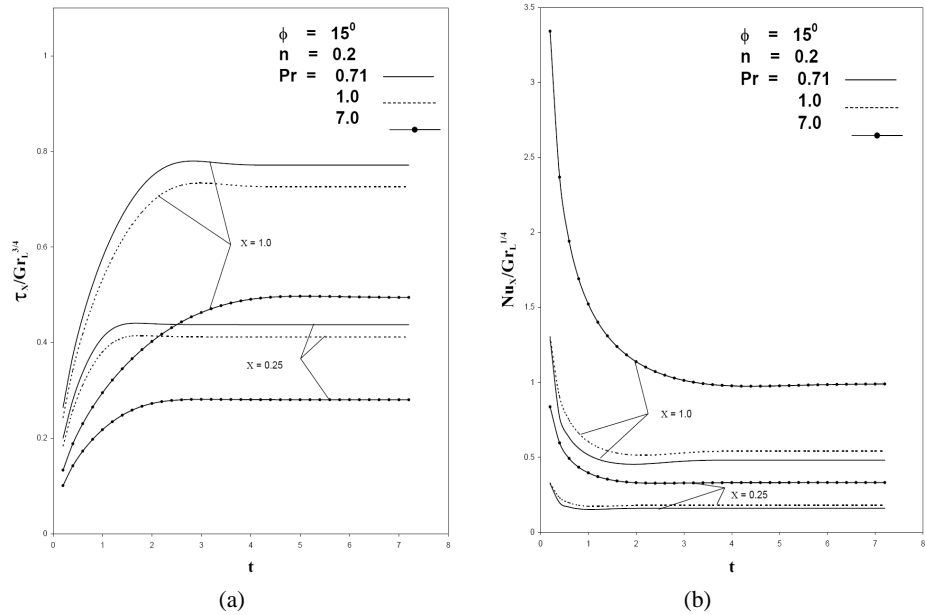


Fig. 7. Local skin friction (a) and local Nusselt number (b) at $X = 0.25$ and 1.0 for different values of Pr in transient period.

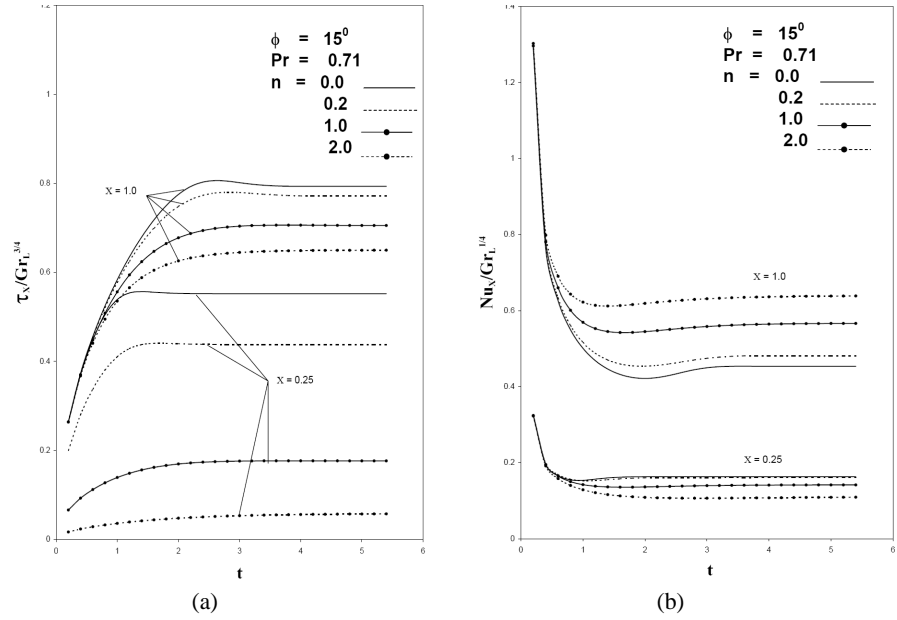


Fig. 8. Local skin friction (a) and local Nusselt number (b) at $X = 0.25$ and 1.0 for different values of n in transient period.

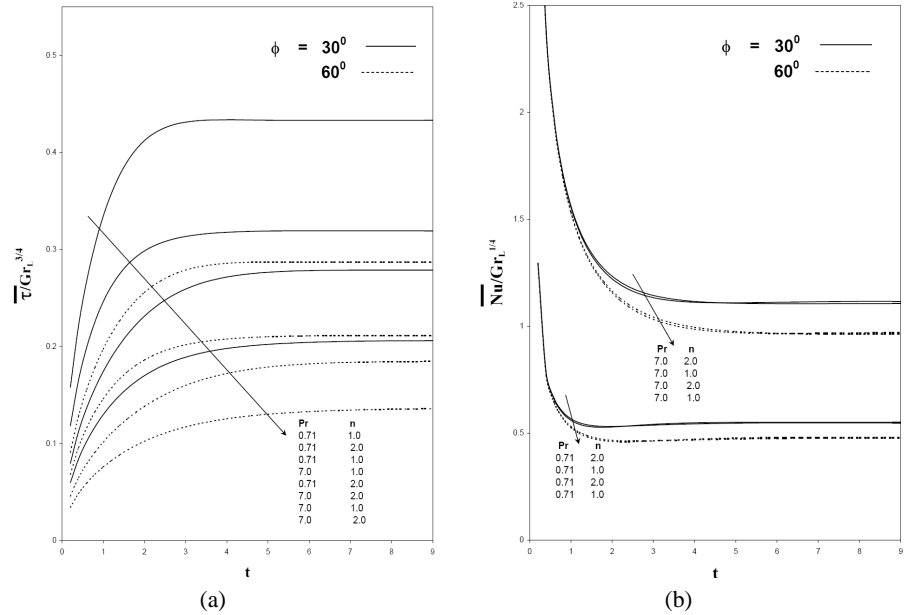


Fig. 9. Average skin friction (a) and average Nusselt number (b) for different values of Pr , n , and ϕ in transient period.

5 Conclusions

This paper deals with the flow over an unsteady non-isothermal vertical cone. The dimensionless governing boundary layer equations are solved by an implicit finite-difference method of Crank-Nicolson type. Present results are compared with available results in literature and are found to be in good agreement. The following conclusions are made:

1. The velocity reduces when the parameters ϕ , Pr , n are increased.
2. Temperature increases with increasing ϕ and decreasing Pr , n values.
3. Momentum boundary layers become thick when ϕ and Pr are increased.
4. Thermal boundary layer becomes thin when ϕ is reduced and Pr is increased.
5. The time taken to reach steady state increases with increasing ϕ , Pr and n .
6. The difference between temporal maximum velocity value and steady state value becomes more when ϕ , Pr , and n are decreased.
7. Decreasing ϕ or increasing Pr , n reduces the difference between temporal maximum temperature values and steady state values.
8. The influence of n over the local skin friction τ_X is large near the apex of the cone and that reduces slowly with increasing distance from it but, for the values of ϕ , Pr the local skin friction τ_X is less near the apex of the cone and that become more with increasing distance from it.
9. The effect of the local Nusselt number Nu_X is less near the cone apex for the values of ϕ , Pr . In transient period, the local Nusselt number Nu_X reduces with increasing n near the apex but that trend is changed and reversed as the distance increases from it.
10. Average skin friction $\bar{\tau}$ is increases when the values of ϕ , Pr , n are reduced and average Nusselt number \overline{Nu} is reduces when the values of Pr decreased or ϕ increased. The effect of n on average Nusselt number \overline{Nu} is almost negligible.

References

1. H. J. Merk, J. A. Prins, Thermal convection laminar boundary layer-I, *Appl. Sci. Res. A*, **4**, pp. 11–24, 1953.
2. H. J. Merk, J. A. Prins, Thermal convection laminar boundary layer-II, *Appl. Sci. Res. A*, **4**, pp. 195–206, 1954.
3. W.H. Braun, S. Ostrach, J.E. Heighway, Free convection similarity flow about two-dimensional and axi-symmetric bodies with closed lower ends, *Int. J. Heat Mass Transfer*, **2**, pp. 121–135, 1961.

4. R. G. Hering, R. J. Grosh, Laminar free convection from a non-isothermal cone, *Int. J. Heat Mass Transfer*, **5**, pp. 1059–1068, 1962.
5. R. G. Hering, Laminar free convection from a non-isothermal cone at low Prandtl number, *Int. J. Heat Mass Transfer*, **8**, pp. 1333–1337, 1965.
6. E. M. Sparrow, L. De Mello, F. Guinle, Deviation from classical free convection boundary layer theory at low Prandtl numbers, *Int. J. Heat Mass Transfer*, **11**, pp. 1403–1406, 1968.
7. S. Roy, Free convection from a vertical cone at high Prandtl numbers, *Trans. ASME Journal of Heat Transfer*, **96**, pp. 115–117, 1974.
8. M. Alamgir, Overall heat transfer from vertical cones in laminar free convection: an approximate method, *ASME Journal of Heat Transfer*, **101**, pp. 174–176, 1989.
9. I. Pop, H. S. Takhar, Compressibility effects in laminar free convection from a vertical cone, *Applied Scientific Research*, **48**, pp. 71–82, 1991.
10. M. Kumari, I. Pop, G. Nath, Mixed convection along a vertical cone, *Int. Comm. Heat Mass Transfer*, **16**, pp. 247–255, 1989.
11. I. Pop, T. Grosan, M. Kumari, Mixed convection along a vertical cone for fluids of any Prandtl number case of constant wall temperature, *Int. J. of Numerical Methods for Heat & Fluid Flow*, **13**, pp. 815–829, 2003.
12. R. S. R. Gorla, R. A. Startman Natural convection boundary layer flow of water at past slender cones, *Int. Comm. Heat Mass Transfer*, **13**, pp. 403–411, 1986.
13. H. K. Kuiken, Axisymmetric free convection boundary-layer flow past slender bodies, *Int. J. Heat Mass Transfer*, **11**, pp. 1141–1153, 1968.
14. T. Watanabe, Free convection boundary layer flow with uniform suction injection over a cone, *Acta Mechanica*, **87**, pp. 1–9, 1991.
15. M. A. Hossain, S. C. Paul, Free convection from a vertical permeable circular cone with non-uniform surface temperature, *Acta Mechanica*, **151**, pp. 103–114, 2001.
16. H. S. Takhar, A. J. Chamkha, G. Nath, Effect of thermo-physical quantities on the natural convection flow of gases over a vertical cone, *Int. J. Engineering Science*, **42**, pp. 243–256, 2004.
17. H. S. Takhar, P. Ganesan, K. Ekambavanan, V. M. Soundalgekar, Transient free convection past a semi-infinite vertical plate with variable surface temperature, *Int. J. Numerical Methods for Heat & Fluid Flow*, **7**, pp. 280–296, 1997.
18. R. Muthucumaraswamy, P. Ganesan, Finite difference solution of flow past an impulsively started vertical plate with variable surface temperature, *Differential Equations and Dynamical Systems*, **7**, pp. 419–436, 1999.
19. K. Ekambavanan, P. Ganesan, Finite difference solution of unsteady natural convection boundary layer flow over an inclined plate with variable surface temperature, *Wrme-und Stoffbertr.*, **30**, pp. 63–69, 1994.
20. P. Ganesan, H. P. Rani, Transient natural convection flow over vertical cylinder with variable surface temperature, *Forschung im Ingenieurwesen*, **66**, pp. 11–16, 2000.
21. B. Carnahan, H. A. Luther, J. O. Wilkes, *Applied Numerical Methods*, John Wiley and Sons, New York, 1969.